



Constructing nitrogen doped graphene quantum dots-ZnNb₂O₆/g-C₃N₄ catalysts for hydrogen production under visible light



Ming Yan^a, Yinquin Hua^a, Fangfang Zhu^b, Lin Sun^b, Wei Gu^b, Weidong Shi^{b,*}

^a School of Material Science and Engineering, Jiangsu University, Zhenjiang 212013, China

^b School of Chemistry and Chemical Engineering, Jiangsu University, Zhenjiang 212013, China

ARTICLE INFO

Article history:

Received 21 September 2016

Received in revised form 18 January 2017

Accepted 24 January 2017

Available online 24 January 2017

Keywords:

NGQDs-ZnNb₂O₆/g-C₃N₄

Heterostructures

Hydrogen

Photocatalysts

ABSTRACT

The development of efficient visible-light-driven photocatalysts for water splitting has drawn much attention. Herein, we demonstrated a novel H₂-producing photocatalytic system that employed nitrogen doped graphene quantum dots (NGQDs)-ZnNb₂O₆/g-C₃N₄ heterostructures as the hydrogen evolving catalysts. The as-prepared NGQDs-ZnNb₂O₆/g-C₃N₄ heterostructures were favorable for light harvesting and charge separation, and showed highly efficient photocatalytic performance for water splitting into hydrogen. Results showed that both the ZnNb₂O₆/g-C₃N₄ (Zn/CN) mole ratio and the amount of NGQDs displayed important influence for H₂ production. Moreover, the optimum synthesis conditions of the Zn/CN mole ratio (1/7) and the amount of NGQDs (5%) were both obtained, and the corresponding 5%NGQDs-Zn₇CN sample performed a much higher hydrogen-evolution rate of 340.9 μmol h⁻¹ g⁻¹. By the further studies, the enhanced photocatalytic activity could be ascribed to the crucial roles of NGQDs and heterojunction photocatalytic system, which resulted in an efficient charge separation and the largely enhanced photocatalytic activity. Meanwhile, the possible photocatalytic mechanism of NGQDs-ZnNb₂O₆/g-C₃N₄ was also proposed. We envision that this work creates new opportunities for constructing and designing efficient visible-light-driven photocatalysts for hydrogen evolution reaction.

© 2017 Published by Elsevier B.V.

1. Introduction

Energy deficiency for human society is an emergency issue now. It is generally believed that hydrogen energy is an ideal candidate for the replacement energy resources, due to its recycling possibility and environmental friendliness [1–3]. Recently, utilizing solar energy for H₂ production from water splitting has proven to be extremely challenging, and the key issue is centered on the efficient conversion of solar energy into chemical energy with lower cost and energy consumption [4–6]. It is well known that the two half reactions of water splitting, the oxygen evolution reaction (OER: 2H₂O → O₂ + 4H⁺ + 4e⁻) and the hydrogen evolution reaction (HER: 2H⁺ + 2e⁻ → H₂), both request catalysts to occur during practical rates. Therefore, development of efficient and facile water splitting photocatalysts is of particular interest in energy studies. However, the stable and efficient photocatalysts, which are capable of absorb-

ing visible-light for an optimized use of solar energy, are still very prerequisite [7,8].

Recently, the metal-free and graphite-like photocatalyst, polymeric graphitic carbon nitride (g-C₃N₄) with outstanding chemical and thermal stability, has attracted considerable interest, because its conduction was sufficient for water reduction to produce hydrogen [9–12]. However, the photocatalytic reaction over single g-C₃N₄ still faces the invalidation owing to its the high excitation binding energy and low hydrogen yield, which is often considered as a major barrier in the single-component semiconductor photocatalyst. In this regard, various effective methods had been developed to improve catalytic performance, such as constructing semiconductor heterojunctions by combining two different catalysts with valence bands and suitable conduction, doping with metal/non-metal, and creating nanoarchitectures [13–18]. Indeed, constructing a heterojunction photocatalytic system, which can efficiently improve the rate of electron-hole pair separation, is vitally momentous for hydrogen production. Since pioneering contributions by the research groups from Wang, the manipulation of composite heterojunctions coupled with g-C₃N₄ has been exten-

* Corresponding author.

E-mail address: swd1978@ujs.edu.cn (W. Shi).

sively developed and designed for water splitting catalysts, such as ZnS and CdS [19,20].

On the one hand, ZnNb_2O_6 , with a columbite structure, has gained considerable interest owing to its applications in photoluminescence, microwave dielectric, and photocatalysis [21–24]. Importantly, the conduction band of ZnNb_2O_6 is also suitable for H_2 production. Therefore, it can be speculated that constructing ZnNb_2O_6 with $\text{g-C}_3\text{N}_4$ may provide a feasible solution to deal with its drawbacks of low efficiency. On the other hand, as a class of one- or few-layered graphene sheets with the size smaller than 10 nm, graphene quantum dots (GQDs) have been applied in the fields of electrochemical biosensors, drug delivery, bioimaging, and energy conversion owing to their unique edge effects and quantum confinement [25–29]. The quantum effect endowed GQDs with broad-band optical absorption. Thus, the GQDs were widely used as light absorbers to couple with semiconductor nanoparticles [30,31]. Meanwhile, both theoretical and experimental researches have indicated that when the nitrogen atoms were introduced into the carbon lattice of quantum dots (NGQDs), both electronic property and chemical reactivity will be tailored [32–34]. Hence, we envision that the NGQDs can be regarded as an ideal light absorber, which will increase visible-light harvesting capability of photocatalysts and generate more electrons-holes pairs.

Here we introduced a type of simple and effective strategy for the synthesis of NGQDs- $\text{ZnNb}_2\text{O}_6/\text{g-C}_3\text{N}_4$ heterojunction by using the hydrothermal reaction, which could be used as an efficient photocatalyst for visible-light-driven H_2 generation from water splitting. Specifically, the influence of the relative amount of the ZnNb_2O_6 , $\text{g-C}_3\text{N}_4$ and NGQDs for photocatalytic hydrogen production in methanol aqueous solutions was systematically studied. Moreover, the possible mechanism toward the photocatalysis process of NGQDs- $\text{ZnNb}_2\text{O}_6/\text{g-C}_3\text{N}_4$ had also been proposed and discussed in detailed. The introduction of NGQDs could be functioned as light absorbers to excited $\text{g-C}_3\text{N}_4$ to generate more electron-hole pairs, and the photoinduced electrons from $\text{g-C}_3\text{N}_4$ could easily inject into the ZnNb_2O_6 , thus leading to an enhancement of photocatalytic performance. As a result, we envision that the as-prepared composite heterojunction structures will provide new insights for designing overall water splitting catalysts.

2. Experimental section

2.1. Materials

Niobium pentoxide (Nb_2O_5), potassium hydroxide (KOH), zinc nitrate ($\text{Zn}(\text{NO}_3)_2 \cdot 6\text{H}_2\text{O}$), urea, ammonium citrate ($\text{C}_6\text{H}_5\text{O}_7(\text{NH}_4)_3$), sodium hydroxide (NaOH) were purchased from Sinopharm Chemical Reagent. All chemicals were of analytical reagent grade and used without further purification, deionized water was used in all experiments.

2.2. Synthesis of NGQDs- $\text{ZnNb}_2\text{O}_6/\text{g-C}_3\text{N}_4$ heterojunction photocatalysts

The $\text{g-C}_3\text{N}_4$ were prepared according to the previous literature [35]. A certain amount of urea was placed the alumina crucible with a lidded, then heated at 550 °C for 2 h. After cooling naturally to room temperature, the resultant powder was then direct heated to 550 °C for 2 h. In a typical procedure for the synthesis of NGQDs, 1 g $\text{C}_6\text{H}_5\text{O}_7(\text{NH}_4)_3$ and 20 mL of H_2O were put into a beaker and heated to 200 °C with an oil bath pan for 30 min. Finally, the pH was adjusted to 7 with NaOH (10 mg/mL) solution. The NGQDs- $\text{ZnNb}_2\text{O}_6/\text{g-C}_3\text{N}_4$ samples were prepared as follows. Firstly, 0.5 g Nb_2O_5 and 3.37 g KOH were added in the 60 mL of distilled water and then transferred into a 100 mL

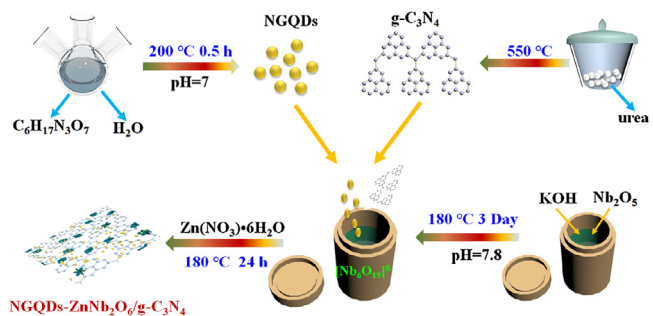


Fig. 1. Schematic illustration for the synthesis of NGQDs- $\text{ZnNb}_2\text{O}_6/\text{g-C}_3\text{N}_4$ heterojunction photocatalysts.

Teflon-lined stainless steel autoclave at 180 °C for 3 days. After cooling naturally, the clear solution of $[\text{Nb}_6\text{O}_{19}]^{8-}$ was obtained. Secondly, 10 mL of distilled water were added into 10 mL of $[\text{Nb}_6\text{O}_{19}]^{8-}$ solution and the pH was adjusted to 7.8 by the addition of HCl solution. Then, X (0.33, 1, 1.65, 2.3 and 3) mmol $\text{g-C}_3\text{N}_4$ powers were added to above solution with continuous stirring for 30 min. Subsequently, 0.1 g $\text{Zn}(\text{NO}_3)_2 \cdot 6\text{H}_2\text{O}$ was added under continuous stirring for another 30 min (abbreviated as Zn/CN, Zn/3CN, Zn/5CN, Zn/7CN and Zn/9CN). After that, different amount of the NGQDs were dissolved in above solution with continuous stirring for 60 min. The preparation of NGQDs- $\text{ZnNb}_2\text{O}_6/\text{g-C}_3\text{N}_4$ with different starting mass ratios of NGQDs to $\text{ZnNb}_2\text{O}_6/\text{g-C}_3\text{N}_4$ (0.01, 0.03, 0.05 and 0.07) were labeled as 1%NGQDs- $\text{ZnNb}_2\text{O}_6/\text{g-C}_3\text{N}_4$, 3%NGQDs- $\text{ZnNb}_2\text{O}_6/\text{g-C}_3\text{N}_4$, 5%NGQDs- $\text{ZnNb}_2\text{O}_6/\text{g-C}_3\text{N}_4$ and 7%NGQDs- $\text{ZnNb}_2\text{O}_6/\text{g-C}_3\text{N}_4$. Finally, the obtained precursor was transferred into a Teflon-lined stainless autoclave at 180 °C for 24 h. The products were filtered, washed with distilled water, and dried at 60 °C for 12 h. The synthesis process was schematically illustrated in Fig. 1.

2.3. Catalyst characterization

The phase purity and crystal structure of the obtained photocatalysts were measured by X-ray diffraction (XRD) using a D/MAX-2500 diffract meter (Rigaku, Japan) with a nickel-filtered $\text{Cu K}\alpha$ radiation source ($\lambda = 1.54056 \text{ \AA}$). The X-ray photoelectron spectroscopy (XPS) was obtained by a Thermo ESCALAB 250X (America) electron spectrometer using 150WAl Ka X-ray sources. Scanning electron microscopy (SEM) was obtained by the Hitachi S-4800 field emission SEM (FESEM, Hitachi, Japan) to observe the morphology of the as-prepared samples. Transmission electron microscopy (TEM) and high-resolution transmission electron microscopy (HRTEM) were gathered on an F20 S-TWIN electron microscope (Tecnai G2, FEI Co.), equipping with a 200 kV accelerating voltage. UV-vis absorption spectra (DRS) were collected using a Shimadzu UV-vis 2550 spectrophotometer. BaSO_4 was used as a reflectance standard material. The photoluminescence (PL) spectra was obtained on a F4500 (Hitachi, Japan) photoluminescence detector. The Fourier transform infrared spectra (FT-IR) of the materials were analyzed using Nicolet Nexus 470 spectrometer.

2.4. Photoelectrochemical measurements

Photocurrent tests were carried out in a conventional three electrode system on the CHI852C electrochemical workstation by using 0.5 M Na_2SO_4 electrolyte, and the irradiation area was 1 cm^2 under 150 W xenon lamp. A Pt foil as the counter electrode and an Ag/AgCl electrode as a reference electrode. The working electrodes were prepared as follows: 10 mg of the as-prepared sample was dispersed into 1 mL ethanol 1 mL ethylene glycol to produce a suspension, which was then coated onto a $1.5 \times 3 \text{ cm}^2$ FTO glass

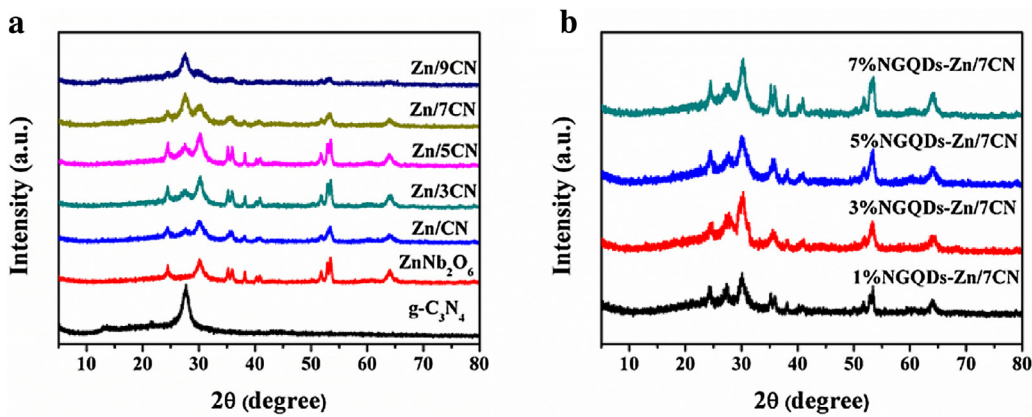


Fig. 2. XRD patterns of as-prepared samples.

electrode. Electrochemical impedance spectroscopy (EIS) measurements were carried out in a three electrode electrochemical cell on a CHI760E electrochemical workstation. A 0.1 M KCl solution containing 5 mM Fe(CN)₆^{3-/4-} was used as the electrolyte.

2.5. Photocatalytic hydrogen production

The photocatalytic H₂ production reaction was conducted in a Lab-H₂ photocatalytic system. The light source was vertically placed on the top of the reactor with a 300 W xenon arc lamp equipped with an optical filter ($\lambda > 420$ nm). 50 mg powder catalysts were suspended in 200 mL of a 20% methanol aqueous solution and stirred continuously to ensure uniform irradiation of the catalyst suspension. 1% noble metals Pt was loaded onto the surface of the photocatalyst by a photochemical reduction deposition method using H₂PtCl₆. The reaction temperature of the reactant solution was maintained at 273 K. The amount of H₂ production was collected with analyzed by gas chromatograph at room temperature (GC-14C, Shimadzu, Japan, TCD, with argon as a carrier gas) once half hour.

3. Results and discussion

3.1. Characterization of the NGQDs

Fig. S1a showed the TEM image of pure NGQDs with the size was about 5–10 nm. XPS measurement was carried out to examine the chemical composition of the as-synthesized NGQDs. As shown in Fig. S1b, three predominant peaks at 284.0 eV, 400.0 eV and 530.6 eV should be ascribed to the C 1s, N 1s and O 1s, respectively. The C1 s in Fig. S1c was divided into five peaks at 284.6 eV, 285.2 eV, 286.6 eV, 287.3 eV and 289.0 eV, which corresponded to C–C, C–N, C–O, C=O and O=C=O, respectively [36–38]. From Fig. S1d, the peak of N 1s binding energies at 398.1 eV, 399.2, 400.5 eV and 401.9 eV could be ascribed to pyridinic-like N, pyrrolic-like N, graphitic-like N and N–H, respectively [39–41]. Based on the as-obtained XPS results, it can be concluded that N atoms were successfully introduced into the QDs.

3.2. Structure and morphology

XRD patterns were then carried out to investigate the crystalline phase structure of as-prepared samples. As shown in Fig. 2a, the diffraction peaks were located at 13.1° and 27.4°, corresponding to the (100) and (002) planes of g-C₃N₄ (JCPDS 87-1526). Meanwhile, all the bands were identified to the diffraction bands from the columbite ZnNb₂O₆ (JCPDS No. 76-1827). With respect to the ZnNb₂O₆/g-C₃N₄ composites, the peak intensities of g-C₃N₄

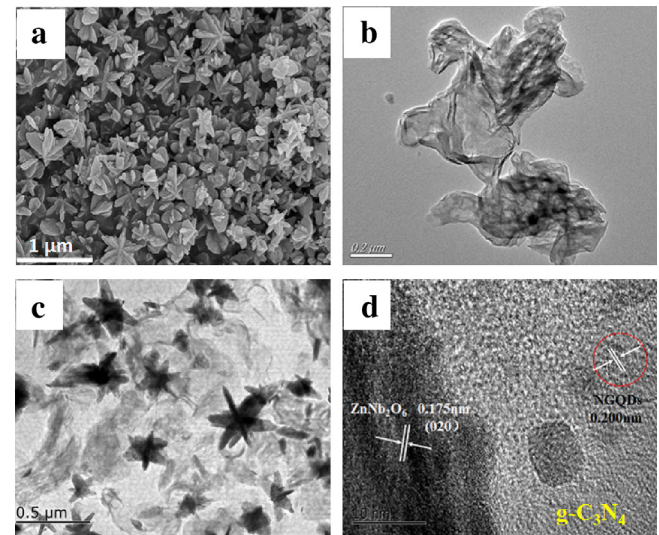


Fig. 3. SEM images of ZnNb₂O₆ (a, b), TEM images of g-C₃N₄ (c) and 5%NGQDs-Zn/7CN (d, e), HRTEM image of 5%NGQDs-Zn/7CN (f).

became stronger as increasing the content of g-C₃N₄. However, when the NGQDs were introduced on the surface of Zn/7CN in Fig. 2b, there was no obvious diffraction peaks of NGQDs, which could be attributed to the low loading amount and low crystallinity of NGQDs.

The morphology information of as-prepared samples was investigated by SEM and TEM. Fig. 3a showed the ZnNb₂O₆ with a uniform hexagonal flower structure. The g-C₃N₄ exhibited the thin and irregular nanosheets (Fig. 3b), which was agreement with the typical structural characteristic of graphite-like carbon nitride. The HRTEM of ZnNb₂O₆/g-C₃N₄ was provided in Fig. S2, it can be observed that the ZnNb₂O₆ integrated compactly on g-C₃N₄ surface with an intimate interface, which was benefit for electron transfer. For composites, we selected the representative sample of 5%NGQDs-Zn/7CN which exhibited the highest photocatalytic activity to investigate the morphology characteristic. In Fig. 3c, the TEM images of the 5%NGQDs-Zn/7CN sample showed that the ZnNb₂O₆ and g-C₃N₄ were close enough and mixed with each other. Meanwhile, there were many dark dots could be found in Fig. 3d and most of them were adhering to the surface of g-C₃N₄, which provided a strong evidence for explaining the existence of NGQDs. The instinct lattice fringe of 0.200 nm corresponded to the NGQDs, which was accordant with that of the graphite carbon source [36]. In addition, the clear lattice fringed with a d-spacing of 0.175 nm, corresponding to the (020) plane of ZnNb₂O₆.

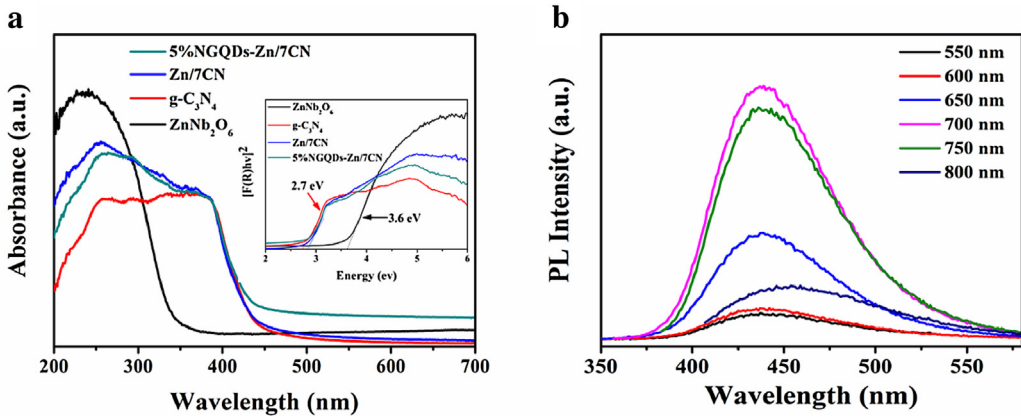


Fig. 4. UV-vis adsorption spectra with as-prepared samples (a), Up-converted PL spectra of NGQDs (b).

The Raman absorption spectra of the ZnNb_2O_6 , $\text{g-C}_3\text{N}_4$, $\text{Zn}/7\text{CN}$ and 5%NGQDs-Zn/7CN were exhibited in Fig. S3. Compared to $\text{Zn}/7\text{CN}$, the 5%NGQDs-Zn/7CN hybrids materials displayed two relatively obvious peaks at 1382 cm^{-1} and 1585 cm^{-1} , corresponding to the D band and G band of NGQDs, respectively. This results suggested that the NGQDs had been coupled together successfully.

3.3. UV-vis absorption spectra and up-converted PL spectra

The excellent optical absorption feature of catalysts played an important role in enhancing its photocatalytic performance [42,43]. The UV-vis diffuse reflectance spectroscopy of the ZnNb_2O_6 , $\text{g-C}_3\text{N}_4$, $\text{Zn}/7\text{CN}$ and 5% NGQDs-Zn/7CN samples were characterized to investigated their optical properties. As shown in Fig. 4a, pure ZnNb_2O_6 possessed absorption edge at around 345 nm, which corresponded to the band gap energy of 3.6 eV. While bare $\text{g-C}_3\text{N}_4$ had the sharp absorption edge at about 460 nm, which corresponded to the band gap energy of 2.7 eV. For the $\text{Zn}/7\text{CN}$ sample (the mixture of ZnNb_2O_6 and $\text{g-C}_3\text{N}_4$ samples with the mole ratio of 1:7), the absorption within the visible light range apparently appeared a red shift compared with pure ZnNb_2O_6 , which suggested that the $\text{Zn}/7\text{CN}$ composites possessed good visible light response. When the 5% NGQDs were introduced into the $\text{Zn}/7\text{CN}$ sample, the light absorption intensity could be clearly enhanced. In addition, with increasing the NGQDs content exceed 5%, the absorption intensity would be further improved in Fig. S4. The UV-vis results suggested that the heterojunction contractures ($\text{ZnNb}_2\text{O}_6/\text{g-C}_3\text{N}_4$) and NGQDs might play important roles in utilizing sunlight. The enhanced light absorption of NGQDs-ZnNb₂O₆/g-C₃N₄ samples were beneficial to generate more electron-hole pairs.

In order to explored the optical property of NGQDs, the up-converted PL spectra was investigated using different excitation wavelengths ranging from 550 to 800 nm in Fig. 4b. It can be clearly observed that NGQDs can absorb visible light (550–800 nm) then emitted photoluminescence at a shorter wavelength (400–500 nm). Thus, the NGQDs can convert visible light to shorter wavelengths for exciting $\text{g-C}_3\text{N}_4$, leading to $\text{g-C}_3\text{N}_4$ photocatalyst can effectively harness the broad spectrum of sunshine and then enhance the photocatalytic performance of NGQDs-ZnNb₂O₆/g-C₃N₄.

The energy band positions of ZnNb_2O_6 and $\text{g-C}_3\text{N}_4$ can be calculated with the following equation [44]:

$$E_{CB} = X - E^e - 0.5E_g$$

$$E_{VB} = E_{CB} + E_g$$

where E^e is the energy of free electrons on the hydrogen scale (4.5 eV), X is the electronegativity of the semiconductor (X value for ZnNb_2O_6 is 6.18 and for $\text{g-C}_3\text{N}_4$ is 4.73), which is the geometric mean of the electronegativity of the constituent atoms. Based on the UV-vis diffuse reflectance absorption spectra, we know that the band gaps of ZnNb_2O_6 and $\text{g-C}_3\text{N}_4$ were 3.6 eV and 2.7 eV. Meanwhile, the conduction bands (CB) of ZnNb_2O_6 and $\text{g-C}_3\text{N}_4$ could be calculated to be -0.12 eV and -1.12 eV , and the valence bands (VB) of ZnNb_2O_6 and $\text{g-C}_3\text{N}_4$ were 3.48 eV and 1.58 eV , respectively. Furthermore, the flat band potential (E_{fb}) of ZnNb_2O_6 was also measured by Mott-Schottky curves. As shown in Fig. S5, the slope of linear $1/C^2$ potential curve of ZnNb_2O_6 was positive, which suggesting the ZnNb_2O_6 was an n-type semiconductor. The E_{fb} value was calculated from the intercept of the axis with potential values, which was approximately equal -0.32 V vs. Ag/AgCl, equivalent to -0.12 V vs. standard hydrogen electrode (SHE) at pH 6.8 [45–47]. As we all known, for n-type semiconductor, the CB potential approximately equals to E_{fb} due to their adjacent values. Therefore, the corresponding CB of ZnNb_2O_6 was estimated to be -0.12 V , which was similar to the formula computing.

3.4. Photocatalytic activity

Photocatalytic H_2 production activity of the NGQDs-ZnNb₂O₆/g-C₃N₄ samples was carried out in 20% methyl alcohol solution with 1% Pt as a cocatalyst under a 300 W Xe lamp. As shown in Fig. 5a–b, the $\text{ZnNb}_2\text{O}_6/\text{g-C}_3\text{N}_4$ ratio on the photocatalytic H_2 have important influence, the highest hydrogen evolution rate steadily reached to $223.2\text{ }\mu\text{mol g}^{-1}\text{ h}^{-1}$ with the $\text{Zn}/7\text{CN}$, over two times than that of pure $\text{g-C}_3\text{N}_4$ ($103.7\text{ }\mu\text{mol g}^{-1}\text{ h}^{-1}$). However, further increased the content of $\text{g-C}_3\text{N}_4$ in the heterostructures, the photocatalytic activity would be decreased, which might be attribute to excessive $\text{g-C}_3\text{N}_4$ may act as the recombination center of electrons and holes to consequently restrain the photocatalytic activity. In addition, the influence of NGQDs amount on the photocatalytic H_2 production activity was also investigated by varying NGQDs addition amount from 1% to 7% with the unchanged $\text{Zn}/7\text{CN}$ ratio. It can be observed from Fig. 5c–d, when modified with the NGQDs amount from 1% to 5% on the surface of the $\text{Zn}/7\text{CN}$, the photocatalytic H_2 production rate was increased until $340.9\text{ }\mu\text{mol g}^{-1}\text{ h}^{-1}$, which was about 53% higher than that of $\text{Zn}/7\text{CN}$ sample. However, when the amount of NGQDs loading exceeded 5%, the H_2 evolution rates decreased. In addition, the photocatalytic H_2 production activity and suitable characterizations (XRD, Raman, and FT-IR spectra) of $\text{g-C}_3\text{N}_4$ (H-T $\text{g-C}_3\text{N}_4$) and $\text{g-C}_3\text{N}_4/5\%$ NGQDs (H-T $\text{g-C}_3\text{N}_4/5\%$ NGQDs) with hydrothermal treatment at 180°C 24 h were also investigated in the supporting information (Figs. S3 and S6).

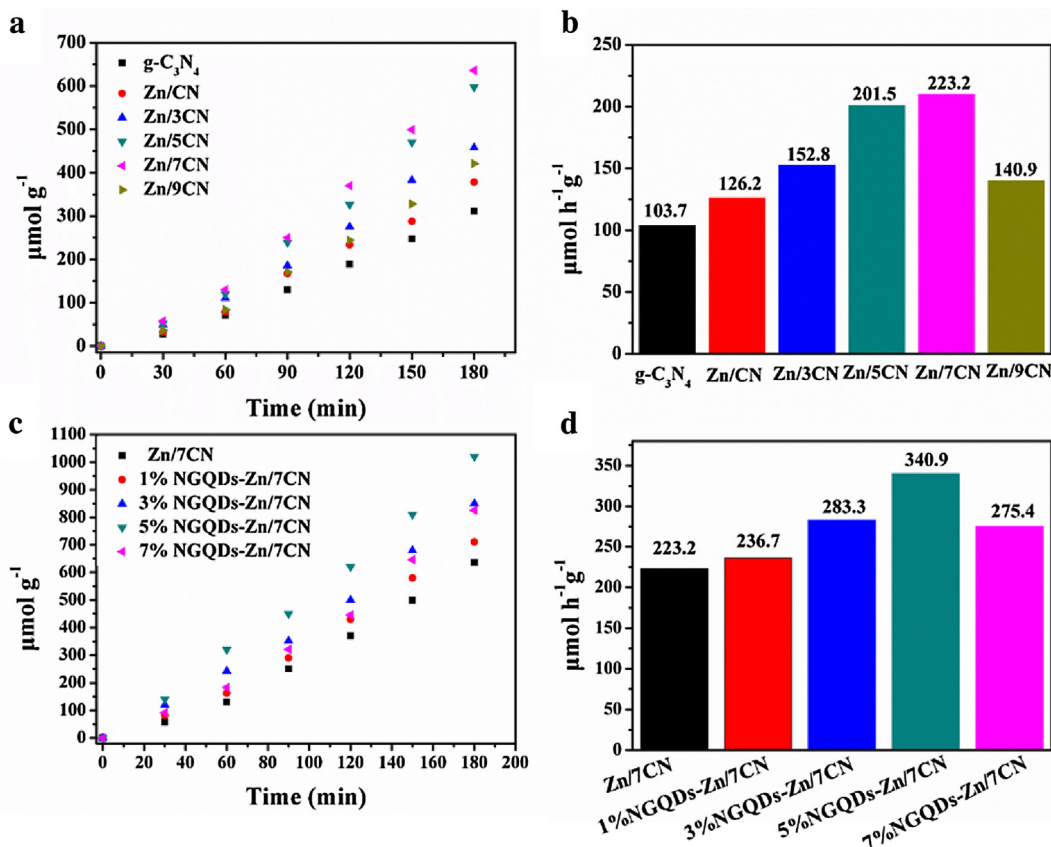


Fig. 5. Plots of photocatalytic H_2 evolution amount visible light irradiation ($\lambda > 420 \text{ nm}$) time for different samples (a and c). Comparison of the visible light induced H_2 evolution rate for different samples (b and d).

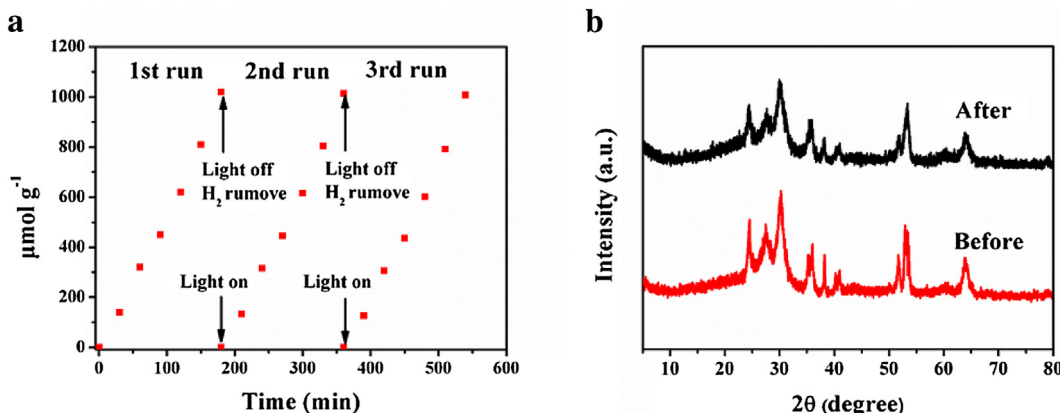


Fig. 6. Stability study of photocatalytic H_2 evolution over 5%NGQDs-Zn/7CN under visible-light irradiation (a). XRD patterns of 5%NGQDs-Zn/7CN before and after 9 h of photocatalytic H_2 evolution reaction.

For the sake of determining the reusability of 5%NGQDs-Zn/7CN photocatalysts, repeating experiment was also carried out. After 9 h irradiation, 335.2 $\mu\text{mol g}^{-1} \text{h}^{-1}$ H_2 was produced without noticeable deactivation, indicating good stability of the catalysts during the photocatalytic reaction (Fig. 6a). It was worth noting that there was no obvious change in material structure after cycle experiments, which was confirmed by the XRD and TEM examination in Figs. 6b and S7 [48–50].

3.5. Electronic and optical properties

The separation efficiency of electrons and holes played a vital role in the photocatalytic reaction. Photoelectrochemical (photo-

currents and EIS) parameters can be used to qualitatively study the separation and transfer of photogenerated charge carriers in photocatalysts. Fig. 7a showed the photocurrent with the ZnNb_2O_6 , $\text{g-C}_3\text{N}_4$, Zn/CN and 5%NGQDs-Zn/7CN samples, it can be seen that the photocurrent intensity of the Zn/7CN exhibited much higher than that of pure ZnNb_2O_6 and $\text{g-C}_3\text{N}_4$, which indicated that a more effective separation of photoinduced electrons and holes and a faster interfacial charge transfer occurred in the Zn/7CN heterostructures. When the Zn/7CN were modified with NGQDs, the NGQDs-Zn/7CN materials displayed much stronger photocurrent. With increasing the content of NGQDs, the photocurrent intensity firstly increased then decreased and the 5%NGQDs-Zn/7CN displayed the highest photocurrent responded (Fig. S8a).

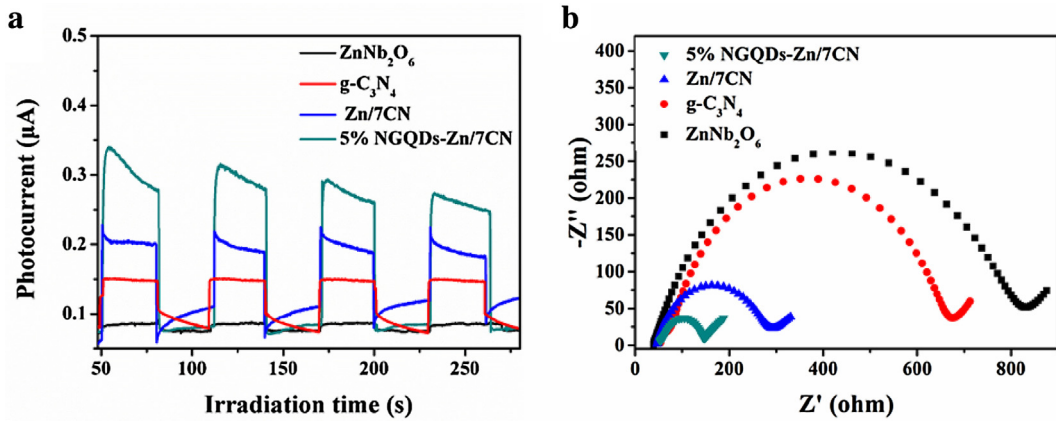


Fig. 7. Transient photocurrent response (a) and EIS (b) for the pure ZnNb_2O_6 , $\text{g-C}_3\text{N}_4$, Zn/7CN and 5%NGQDs-Zn/7CN samples.

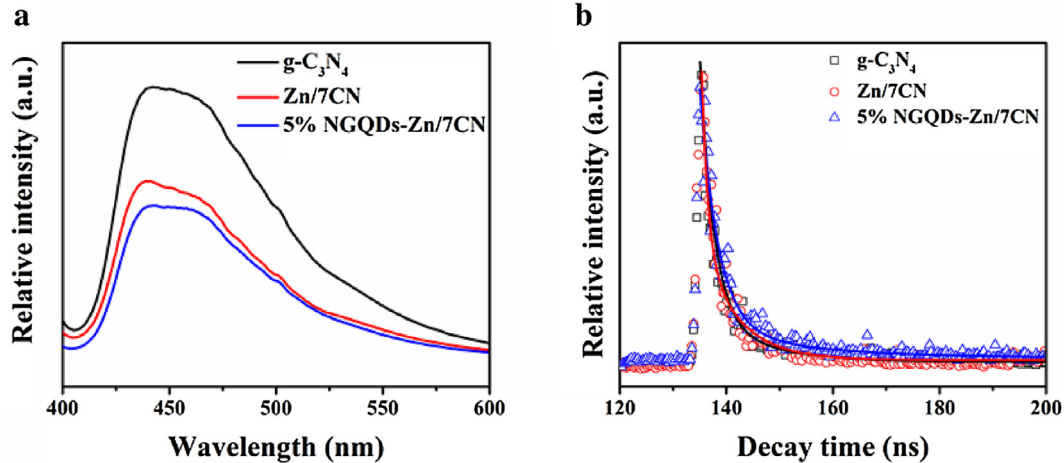


Fig. 8. PL spectra and fluorescence decay curves of the $\text{g-C}_3\text{N}_4$, Zn/7CN and 5%NGQDs-Zn/7CN.

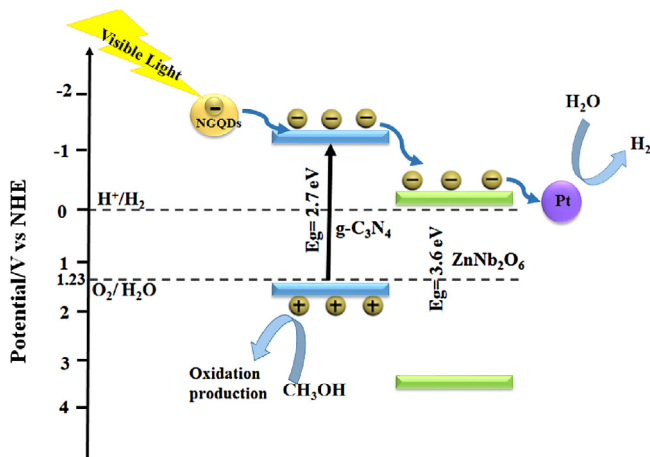


Fig. 9. The proposed photocatalytic H_2 evolution mechanism over NGQDs-ZnNb₂O₆/g-C₃N₄ composites under visible-light irradiation.

The enhanced photocurrent intensity can be attributed to the much more generated photo-generated charge, which indicated the higher separation and transfer efficiency of the photo-induced carriers. Moreover, the EIS was carried out in Figs. 7b and S8b. It can be clearly observed that the 5%NGQDs-Zn/7CN sample displayed the smallest arc radius among all the samples. As we all known, the smaller radius of the Nyquist circle represented faster interfacial charge transfer and a more effective separation of electron

and hole. This result confirmed more photo-generated charge carriers could be separated by the construction of 5%NGQDs-Zn/7CN heterojunction.

Photoluminescence (PL) was employed to further study the recombination abilities of photoexcited electron-hole pairs. A low PL intensity revealed the lower photoinduced charge carriers' recombination. As shown in Fig. 8a, the PL emission intensity of 5%NGQDs-Zn/7CN was the lowest among all the samples with an excitation wavelength at 387 nm, which indicating that the recombination of photogenerated charge carriers was inhibited in the 5%NGQDs-Zn/7CN composite. Fig. 8b showed the fluorescence decay curves of as-prepared samples. The calculated average lifetime values of bare $\text{g-C}_3\text{N}_4$, Zn/7CN and 5%NGQDs-Zn/7CN were 3.15, 3.87 and 5.23 ns, respectively. The conclusions suggested that the 5%NGQDs-Zn/7CN retarded the carriers recombination and enhanced the possibility of charge carriers participating in photocatalytic water splitting [51–54].

3.6. Photocatalytic mechanism

In order to better understanding the pathway of charge transfer, the HRTEM images of $\text{ZnNb}_2\text{O}_6/\text{g-C}_3\text{N}_4$ and NGQDs-ZnNb₂O₆/g-C₃N₄ loading with Pt after the H_2 evolution experiments were also exhibited. As shown in Fig. S9, the Pt particles were deposited on the surface of ZnNb_2O_6 and most NGQDs were adhering to the surface of $\text{g-C}_3\text{N}_4$ (Fig. S9b). On the basis of above discussions and results, it was crucial and necessary to proposed a reasonable and possible photocatalytic H_2 production mechanism. When the

NGQDs-ZnNb₂O₆/g-C₃N₄ sample was subjected to the visible light irradiation (Fig. 9), the NGQDs can absorb light with wavelength ≥ 550 nm and convert them to shorter wavelength <460 nm, which subsequently excited g-C₃N₄ to generate more electron-hole pairs. The photogenerated electrons were excited from the VB to the CB of g-C₃N₄, leaving the holes in the VB of g-C₃N₄. Subsequently, the methanol was oxidized by the positive hole in the g-C₃N₄ VB. Due to the band gap discontinuity, the photoinduced electrons of CB in g-C₃N₄ would inject into the CB of the ZnNb₂O₆. At last, the excited electrons tend to be trapped by the Pt nanoparticles. Hence, the NGQDs-ZnNb₂O₆/g-C₃N₄ remarkably increased charge separation efficiency, leading to an enhancement of photocatalytic performance.

4. Conclusions

In summary, for the first time, we have successfully developed a simple and scalable ternary NGQDs-ZnNb₂O₆/g-C₃N₄ heterojunction which showed exhibited excellent visible-light hydrogen production. The optimum sample of 5%NGQDs-Zn/7CN performed the hydrogen-evolution rate of 340.9 $\mu\text{mol h}^{-1}\text{g}^{-1}$. Importantly, based on the obtained results, the enhancement of activity can be ascribed to the cooperative effects of NGQDs and heterojunction structure, which could generate more electron-holes pairs and accelerate the interfacial charge separation. In general, this study is expected to open up new insights in the development of composite heterojunction photocatalysts and provide some meaningful information for visible-light-driven H₂ generation from water splitting.

Acknowledgements

The authors would like to acknowledge the National Natural Science Foundation of China (21477050 and 21522603), the Chinese German Cooperation Research Project (GZ1091), the Excellent Youth Foundation of Jiangsu Scientific Committee (BK20140011), the Program for New Century Excellent Talents in University (NCET-13-0835), the Henry Fok Education Foundation (141068) and Six Talents Peak Project in Jiangsu Province (XCL-025).

Appendix A. Supplementary data

Supplementary data associated with this article can be found, in the online version, at <http://dx.doi.org/10.1016/j.apcatb.2017.01.070>.

References

- [1] A. Listorti, J. Durrant, J. Barber, *Nat. Mater.* 8 (2009) 929–930.
- [2] D. Kim, K. Sakimoto, D. Hong, P. Yan, *Angew. Chem. Int. Ed.* 54 (2015) 3259–3266.
- [3] H. Li, Y. Zhou, W. Tu, J. Ye, Z. Zou, *Adv. Funct. Mater.* 25 (2015) 998–1013.
- [4] J. Tolleson, *Nature* 464 (2010) 1262–1264.
- [5] D. Gamelin, *Nat. Chem.* 4 (2012) 965–967.
- [6] K. Sanderson, *Nature* 452 (2008) 400–402.
- [7] K. Maeda, K. Teramura, D. Lu, T. Takata, N. Saito, Y. Ioune, K. Domen, *Nature* 440 (2006) 295.
- [8] X. Chen, S. Shen, L. Guo, S. Mao, *Chem. Rev.* 110 (2010) 6503–6570.
- [9] X. Wang, K. Maeda, A. Thomas, K. Takanabe, G. Xin, J. Carlsson, K. Domen, M. Antonietti, *Nat. Mater.* 8 (2008) 76–80.
- [10] X. Wang, K. Maeda, X. Chen, K. Takanabe, K. Domen, Y. Hou, X. Fu, M. Antonietti, *J. Am. Chem. Soc.* 131 (2009) 1680–1681.
- [11] X. Wang, S. Blechert, M. Antonietti, *ACS Catal.* 2 (2012) 1596–1606.
- [12] Y. Wang, X. Wang, M. Antonietti, *Angew. Chem. Int. Ed.* 50 (2011) 2–24.
- [13] X. Wang, X. Chen, A. Thomas, X. Fu, M. Antonietti, *Adv. Mater.* 21 (2009) 1609–1612.
- [14] G. Liu, P. Niu, C. Sun, C. Smith, Z. Chen, G. Lu, H. Cheng, *J. Am. Chem. Soc.* 132 (2010) 11642–11648.
- [15] Z. Lin, X. Wang, *Angew. Chem. Int. Ed.* 52 (2013) 1735–1738.
- [16] G. Zhang, M. Zhang, X. Ye, X. Qiu, S. Lin, X. Wang, *Adv. Mater.* 26 (2014) 805–809.
- [17] Q. Han, C. Hu, F. Zhao, Z. Zhang, N. Chen, *J. Mater. Chem. A* 3 (2015) 4612–4619.
- [18] C.J. Song, M.S. Fan, B. Hu, T.J. Chen, L.P. Wang, W.D. Shi, *CrystEngComm* 17 (2015) 4575–4583.
- [19] J. Zhang, Y. Wang, J. Jin, J. Zhang, Z. Lin, F. Huang, J. Yu, *ACS Appl. Mater. Interfaces* 5 (2013) 10317–10324.
- [20] F. Shi, L. Chen, C. Xing, D. Jiang, D. Li, M. Chen, *RSC Adv.* 4 (2014) 62223–62229.
- [21] S. Ji, S. Choi, J. Jang, E. Kim, J. Lee, *J. Phys. Chem. C* 113 (2009) 17824–17830.
- [22] W. Wu, S. Liang, Z. Ding, H. Zheng, L. Wu, *Solid State Sci.* 13 (2011) 2019–2023.
- [23] Y. Hsiao, T. Fang, L. Ji, *Mater. Lett.* 64 (2010) 2563–2565.
- [24] J. Dai, C. Zhang, L. Shi, W. Song, P. Wu, X. Huang, *Ceram. Int.* 38 (2012) 1211–1214.
- [25] L.L. Li, J. Ji, R. Fei, C.Z. Wang, Q. Lu, J.R. Zhang, *Adv. Funct. Mater.* 22 (2012) 2971–2979.
- [26] D. Qu, M. Zheng, P. Du, Y. Zhou, L.G. Zhang, D. Li, *Nanoscale* 5 (2013) 12272–12277.
- [27] J.Y. Ji, J.L. Liu, L.F. Lai, X. Zhao, Y.D. Zhen, J.Y. Lin, *ACS Nano* 9 (2015) 8609–8616.
- [28] P. Chen, T.Y. Xiao, H.H. Li, J.J. Yang, Z. Wang, H.B. Yao, *ACS Nano* 6 (2012) 712–719.
- [29] L.M. He, L.Q. Jing, Y.B. Luan, L. Wang, H.G. Fu, *ACS Catal.* 4 (2014) 990–998.
- [30] H. Zhang, L.X. Zhao, F.L. Geng, L.H. Guo, B. Wan, Y. Yang, *Appl. Catal. B: Environ.* 180 (2016) 656–662.
- [31] H.T. Li, X.D. He, Z.H. Kang, H. Huang, Y. Liu, J.L. Liu, S.Y. Lian, C.H.A. Tsang, X.B. Yang, S.T. Lee, *Angew. Chem. Int. Ed.* 49 (2010) 4430–4434.
- [32] M. Yan, Y.Q. Hua, F.F. Zhu, W. Gu, J.H. Jiang, H.Q. Shen, W.D. Shi, *Appl. Catal. B: Environ.* 202 (2017) 518–527.
- [33] Y. Li, Y. Zhao, H.H. Cheng, Y. Hu, G.Q. Shi, L.M. Dai, *J. Am. Chem. Soc.* 134 (2012) 15–18.
- [34] Q.Q. Li, S. Zhang, L.M. Dai, L.S. Li, *J. Am. Chem. Soc.* 134 (2012) 18932–18935.
- [35] L.H. Yao, D. Wei, Y.M. Ni, D.P. Yan, C.W. Hu, *Nano Energy* 26 (2016) 248–256.
- [36] Y.Y. Yin, Q. Liu, D. Jiang, X.J. Du, J. Qian, H.P. Mao, K. Wang, *Carbon* 96 (2016) 1157–1165.
- [37] Z. Yang, M.H. Xu, Y. Liu, F.J. He, F. Gao, Y.J. Su, *Nanoscale* 6 (2014) 1890–1895.
- [38] Q.H. Liang, W.J. Ma, Y. Shi, Z. Li, X.M. Yang, *Carbon* 60 (2013) 421–428.
- [39] H.B. Wang, T. Maiyalagan, X. Wang, *ACS Catal.* 2 (2012) 781–794.
- [40] F. Wang, M. Kreiter, B. He, S.P. Pang, C.Y. Liu, *Chem. Commun.* 46 (2010) 3309–3311.
- [41] Q. Li, B.D. Guo, J.G. Yu, J.R. Ran, B.H. Zhang, H.J. Yan, J.R. Gong, *J. Am. Chem. Soc.* 133 (2011) 10878–10884.
- [42] J.X. Xia, J. Di, H.T. Li, H. Xu, H.M. Li, S.J. Guo, *Appl. Catal. B* 181 (2016) 260–269.
- [43] J. Di, J.X. Xia, M.X. Ji, L. Xu, S. Yin, Q. Zhang, Z.G. Chen, H.M. Li, *Carbon* 98 (2016) 613–623.
- [44] M. Yan, Y.L. Wu, Y. Yan, F.F. Zhu, Y.Q. Hua, W.D. Shi, *ACS Sustain. Chem. Eng.* 4 (2015) 757–766.
- [45] X.M. Jia, J. Cao, H.L. Lin, Y. Chen, W.F. Fu, S.F. Chen, *J. Mol. Catal. A: Chem.* 409 (2015) 94–101.
- [46] S.X. Weng, B.B. Chen, L.Y. Xie, Z.Y. Zheng, P. Liu, *J. Mater. Chem. A* 1 (2013) 3068–3075.
- [47] S.N. Sun, W.Z. Wang, D.Z. Li, L. Zhang, D. Jiang, *ACS Catal.* 4 (2014) 3498–3503.
- [48] X.L. Yang, F.F. Qian, G.J. Zou, M.L. Li, J.R. Lu, Y.M. Li, M.T. Bao, *Appl. Catal. B* 193 (2016) 22–35.
- [49] Z.A. Lan, G.G. Zhang, X.C. Wang, *Appl. Catal. B* 192 (2016) 116–125.
- [50] L.Q. Jing, Y.G. Xu, S.Q. Huang, M. Xie, M.Q. He, H. Xu, H.M. Li, Q. Zhang, *Appl. Catal. B* 199 (2016) 11–22.
- [51] D.L. Jiang, T.Y. Wang, Q. Xu, D. Li, S.C. Meng, M. Chen, *Appl. Catal. B* 201 (2017) 617–628.
- [52] X.J. She, J.J. Wu, J. Zhong, H. Xu, Y.C. Yang, R. Vajtai, J. Lou, Y. Liu, D.L. Du, H.M. Li, P. Ajayan, *Nano Energy* 27 (2016) 138–146.
- [53] L. Shi, K. Chang, H.B. Zhang, X. Hai, L.Q. Yang, T. Wang, J.H. Ye, *Small* 12 (2016) 4431–4439.
- [54] K. Li, X. Xie, W.D. Zhang, *Carbon* 110 (2016) 356–366.